Journal of Power Sources 195 (2010) 4593–4599

Contents lists available at ScienceDirect

Journal of Power Sources

journal homepage: www.elsevier.com/locate/jpowsour

Synthesis and evaluation of nano-size lanthanum strontium manganite–yttria-stablized zirconia composite powders as cathodes for solid oxide fuel cells

Jungdeok Park[a], Jing Zou[a], Jongshik Chung[a,b,*]

[a] Department of Chemical Engineering, Pohang University of Science and Technology, San 31, Hyoja-Dong, Nam-Gu, Pohang 790-784, Republic of Korea
[b] School of Environmental Science and Engineering, Pohang University of Science and Technology, San 31, Hyoja-Dong, Nam-Gu, Pohang 790-784, Republic of Korea

ARTICLE INFO

Article history:
Received 14 January 2010
Received in revised form 22 January 2010
Accepted 3 February 2010
Available online 1 March 2010

Keywords:
Solid oxide fuel cell (SOFC)
Lanthanum strontium manganite
Yttria-stablized zirconia
Composite cathode

ABSTRACT

Nano-sized (50 nm) lanthanum strontium manganite ($La_{0.8}Sr_{0.2}MnO_3$, LSM) particles are deposited on yttria-stablized zirconia (8YSZ) by synthesizing LSM particles *in situ* in an YSZ-dispersed solution. As the LSM content is decreased from 80 to 25 wt.%, 50 wt.% powder shows the best microstructure and phase connectivity. This composite, when used as a cathode in a button cell, also has the highest power density of 791 mW cm^{-2} at 800 °C and the lowest values of the cathode polarization resistance and high-frequency arc (0.315 and 0.120 Ω cm^2, respectively). Initially, the low-frequency arc shows a rapid decrease as the LSM content is reduced from 80 to 60 wt.%. After this, an abrupt drop at 50 wt.% LSM content is followed by a slow decrease in the low-frequency arc with further decrease in the LSM content. The results suggest that the high-frequency arc is related to charge transfer and the low-frequency arc to the site density of the triple-phase boundary (TPB). A new parameter, the charge-transfer efficiency of the TPB site, is defined and used to explain further the observed effect of LSM content on YSZ.

1. Introduction

Solid oxide fuel cells (SOFCs) are promising types of fuel cell due to their utilization of less-expensive ceramic materials and their high operating temperatures. Widely used cathode materials in SOFCs are lanthanide transition metal compounds with a perovskite structure. Among them, lanthanum strontium manganite (LSM) is representative because of its chemical stability, electrical conductivity, and compatibility with other cell components. For example, the thermal expansion coefficient of LSM is similar to the popular electrolyte material yttria-stablized zirconia (YSZ), and LSM does not react with YSZ below 1150 °C.

It is known that a combination of electrode material with electrolyte helps to improve the reactivity of the electrode, not only for pure electronic conductors like LSM, but also for mixed conductors, such as LSCF ($La_{1-x}Sr_xCo_{1-y}Fe_yO_3$) [1]. Composite cathodes of LSM–YSZ have been studied by many research groups [2–4], but a dramatic improvement in polarization resistance was observed after the incorporation of YSZ into LSM because the contact points between electrode and electrolyte particles can form an additional triple-phase boundary (TPB). Nanoparticles would be very useful, as they have a large effective surface area which results in an increased TPB. Nanoparticles of perovskite materials developed using co-precipitation, sol–gel or Pechini methods [5–8] have shown improved reactivity in every kind of catalytic reaction. The high surface energy of nanoparticles, however, could induce the agglomeration of particles. Therefore, it would be natural to deposit nanoparticles of the cathode material to the YSZ surface to increase TPB and prevent the agglomeration of cathode particles. In fact, it has already been reported that nano-size LSM particles deposited randomly on the YSZ surface cause an increase in TPB sites and thereby improve performance [9].

In the present study, nanoparticles of LSM are systematically deposited on YSZ particles at different LSM contents by synthesizing LSM particles *in situ* in an YSZ-dispersed solution. The effect of the LSM content on the microstructure and electrochemical properties is investigated to find factors that govern the reactivity of the cathode for oxygen reduction.

2. Experimental

2.1. Synthesis of composite powder

LSM ($La_{0.8}Sr_{0.2}MnO_3$)–YSZ (8 mol.% yttria-stabilized zirconia) composite powders were synthesized by the cellulose–glycine nitrate process (GNP) according to the method employed by Shao

* Corresponding author at: Department of Chemical Engineering, POSTECH, San 31, Hyoja-Dong, Nam-Ku, Pohang 790-784, Korea. Tel.: +82 54 279 2267; fax: +82 54 279 8453.
E-mail address: jsc@postech.ac.kr (J. Chung).

0378-7753/$ – see front matter © 2010 Elsevier B.V. All rights reserved.
doi:10.1016/j.jpowsour.2010.02.069

and co-workers [10]. YSZ powder (Tosho, Japan, less than 2.0 g) was dispersed in 100 ml of distilled water with a high-speed stirrer. $La(NO_3)_3{\cdot}6H_2O$, $Sr(NO_3)_2$, and $Mn(NO_3)_2{\cdot}6H_2O$, with the stoichiometric ratio (Sigma–Aldrich, >99.9%), were added to an aqueous solution containing dispersed YSZ power. Under constant stirring, glycine and activated cellulose (Sigma–Aldrich, >99.9%) were added to the above solution as chelating agents. Two moles of glycine and 75 g of the activated cellulose were used for one mole of total metal cations. To activate the cellulose powder, it was dispersed in nitric acid solution (69 wt.%) for 2 h and then washed with water three times. After glycine addition, the temperature was kept at 80 °C to increase the solution concentration. After the solution turns into a sol, activated cellulose was added. About 2 h later, a black powder was obtained and calcined at 250 °C for 1 h, then 850 °C for 3 h. The weight ratio of LSM:YSZ was varied to obtain seven different composite samples having various LSM contents (25, 33, 45, 50, 60, 70, and 80 wt.%).

2.2. Preparation of cells

To measure the cathodic polarization by means of electrochemical impedance spectroscopy (EIS), a symmetric cell was prepared by coating a slurry solution of cathode powder to both sides of an YSZ pellet using a screen printer. The YSZ pellet, having a size of 17 mm in diameter and 1.1 mm in thickness, was prepared by pressing YSZ powder uniaxially and sintering at 1400 °C for 3 h. The slurry solution of the composite cathode powder was prepared by mixing powder with an ink vehicle (Fuel Cell Materials, USA). The cathode-coated cell was then sintered at 1050 °C for 5 h and the resulting cathode area was kept at 0.20 cm^2. Platinum paste and mesh were attached to the electrode surface to act as the current-collector.

A button cell of the anode support type was fabricated using an anode support that was prepared by pressing a mixture of NiO–YSZ (weight ratio of 55:45) with 35 vol.% graphite (Sigma–Aldrich) and sintering at 1200 °C for 3 h. The anode functional layer (AFL) and the electrolyte layer were coated successively by dipping the anode support into slurries of NiO–YSZ (60:40 wt.%) powder and YSZ powder that were mixed with isopropanol and toluene. Then, the cathode powder slurry of the synthesized LSM–YSZ composite was coated on the electrolyte layer as a cathode functional layer (CFL) by using a screen printer. Finally, a slurry of pure LSM powder was coated on the cathode layer. AFL, CFL and cathode layers were sintered at 1200 °C for 3 h, and the electrolyte layer at 1400 °C for 3 h. The resulting thicknesses of the AFL and electrolyte layers were both about 10 μm, while the cathode area was kept at 0.20 cm^2.

2.3. Characterization of powders

The phase composition of the synthesized powders was identified by means of X-ray diffraction (X-PERT PRO with Cu Kα radiation). The morphology of the powders was observed with a scanning electron microscope (JSM-7401F, JEOL) and a transmission electron microscope (Philips – CM200). The electrochemical properties were characterized by electrochemical impedance spectroscopy (EIS) using a Solartron 1260 frequency response analyzer in an open-circuit state. Impedance spectra were measured in the range of 10 mHz to 100 kHz at five points per frequency decade with a signal amplitude of 10 mV at 800 °C. Using a fitting program, the polarization resistance was calculated. Cell performance was measured with an electronic loader at 800 °C. Hydrogen with 3% water was fed as fuel to the anode and air was fed to the cathode. The fuel and air flow rates were controlled at 15 and 30 mL min^{-1}, respectively.

3. Results and discussion

3.1. Microstructure

The XRD patterns of LSM–YSZ composite cathode powders prepared at various LSM contents (20, 33, 45, 50, 60, 70, and 80 wt.%) are shown in Fig. 1. In all cases, only peaks for LSM (main peak at 32.5°) and YSZ (main peak around 30°) are observed and there are no observed impurity peaks. It is known that La-based perovskite materials react with YSZ electrolytes at temperatures above 1150 °C to form $La_2Zr_2O_7$, which has low electric and ionic conductivity [11–13]. By using Scherrer's equation, a mean crystal size of approximately 20 nm is determined. The TEM images in Fig. 2 show a relatively uniform size of 50 nm for LSM particles and 70–150 nm for the commercial YSZ powder.

The microstructure of the sintered electrode is one of the most important factors in cathode performance. In the composite cathode case, the three-dimensional structure, which is formed by the connection between electrode and electrolyte particles, is a very important part for the cathode reaction. Because LSM is close to a pure electronic conductor, contact points (TPB sites) between the electrode and electrolyte particles ensures both electron and ionic paths to act as reaction sites in the LSM–YSZ composite cathode. The activity was found to be dramatically affected by the incorporation of YSZ [3].

The observed results of TEM and energy-dispersive X-ray spectroscopy (EDS) for composite cathodes with three different LSM contents (80, 50, and 25 wt.%) are presented in Fig. 3. For the LSM-rich sample (80 wt.% content in Fig. 3a), the distribution of YSZ is not uniform, but somewhat localized because an excess amount of LSM allows YSZ particles to separate. For the sample with equal contents of LSM and YSZ (50 wt.% LSM content in Fig. 3b), both LSM and YSZ are uniformly distributed and in close contact with each other. Even when the LSM content is decreased to 20 wt.% (Fig. 3c), the distribution of LSM and YSZ still retains uniformity. This feature is probably due to the smaller size of the LSM particles, which are more or less evenly deposited on larger YSZ particles during the *in situ* synthesis.

Fig. 4 shows the cross-sectional view of the cathode layer in button cells that are manufactured with the three composite cathode materials listed in Fig. 3. For the LSM-rich cathode material (80 wt.% LSM content in Fig. 4a), agglomerated particles that are grown from nanoparticles are tightly packed within small pores. In this case, YSZ particles are probably surrounded by excess LSM particles, which most likely contribute to a reduction in TPB sites

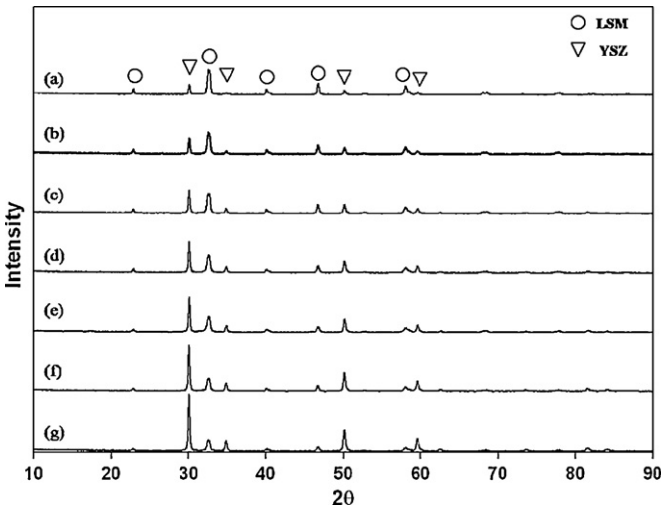

Fig. 1. X-ray patterns of LSM–YSZ composite powders with various LSM contents: (a) 80, (b) 70 (c) 60, (d) 50, (e) 45, (f) 33, (g) 25 wt.%.

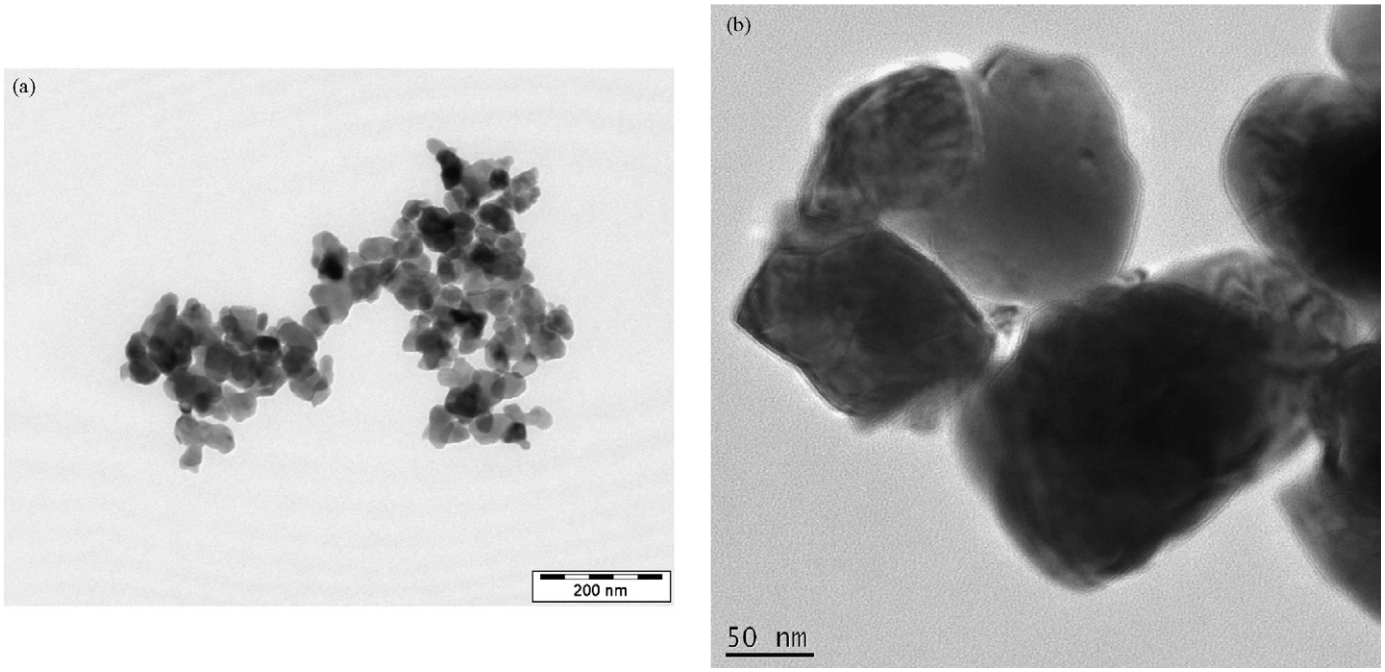

Fig. 2. TEM images of: (a) LSM nano particles, (b) YSZ particles.

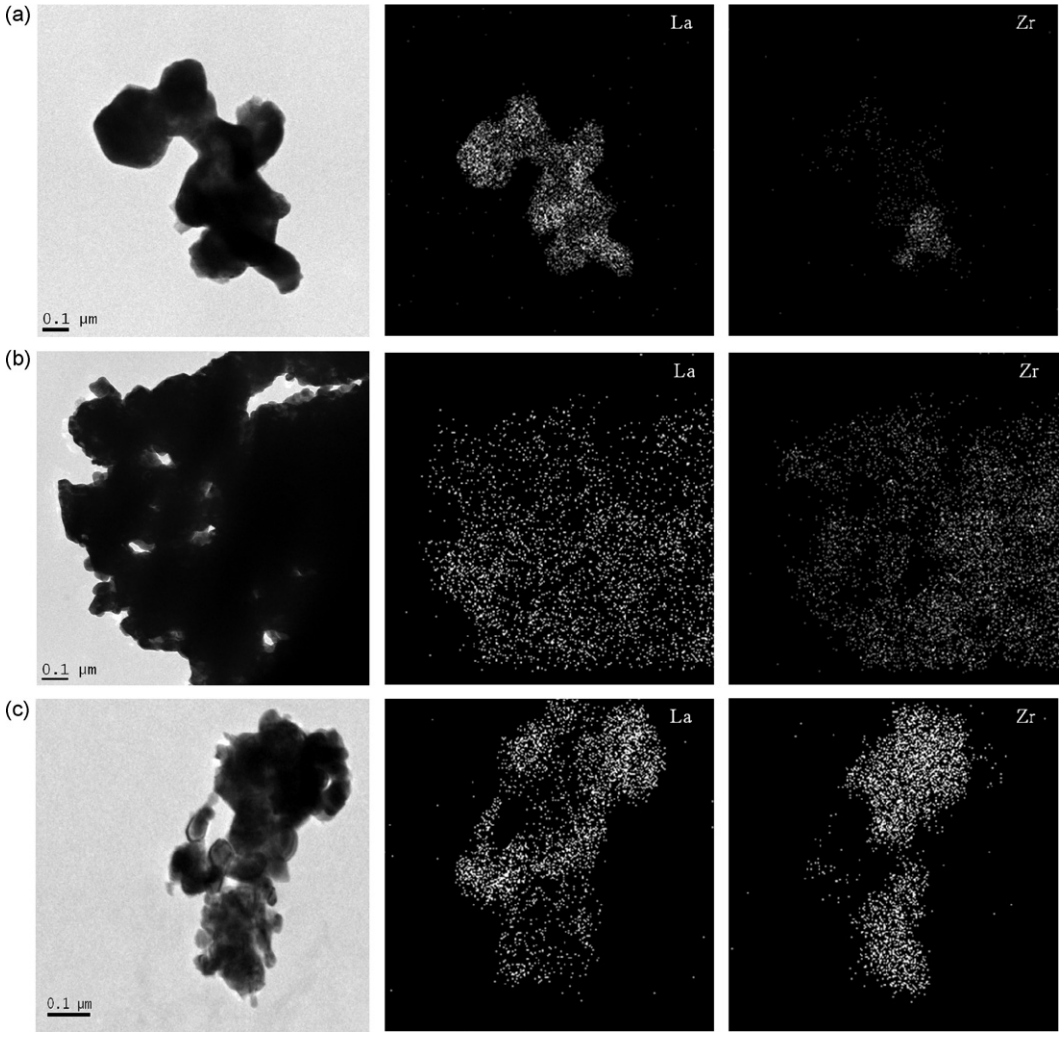

Fig. 3. HR-TEM images and EDS results of LSM–YSZ composite powders with different LSM contents: (a) 80, (b) 50, (c) 25 wt.%.

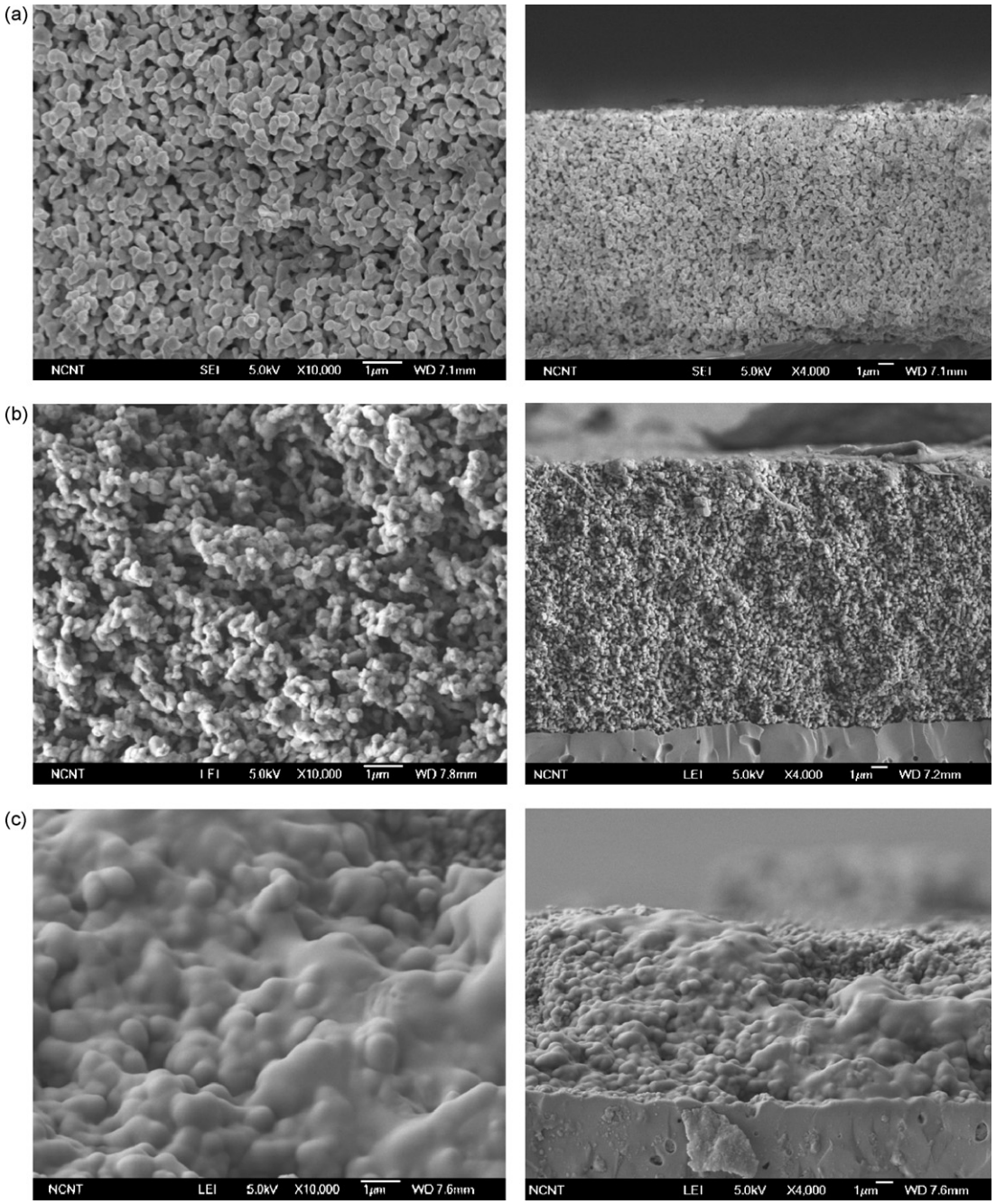

Fig. 4. SEM images of electrode|electrolyte interface of cells fired at 1050 °C for cathodes with various LSM contents: (a) 80, (b) 50, (c) 25 wt.%.

and ionic paths. With 50:50 wt.% of LSM–YSZ (Fig. 4b), particles are smaller and more heterogeneous within larger pores. This structure indicates that LSM and YSZ particles are uniformly distributed and inter-connected with each other. With the lowest LSM content of 20 wt.% in the cathode (Fig. 4c), it is surprising to observe that the particles are in a sintered state with little existence of pores, despite being calcined at the relatively low temperature of 1050 °C. LSM nanoparticles that are doped to the YSZ surface might promote phase connectivity and the eventual sintering of YSZ particles.

3.2. Polarization resistance and cell performance

Many researchers have studied LSM-YSZ composite cathodes by means of EIS measurements [14,15]. Fig. 5 shows the impedance spectra for seven cells of LSM–YSZ composites with different LSM contents. The equivalent circuit $LR_s(QR_{ct})(CR_d)$ was chosen to analyze the impedance spectra [14], in which the R_{ct} and R_d parts are called the high- and low-frequency arcs, respectively. A summary of the results for the polarization resistance (R_p), the high-frequency arc, the low-frequency arc and the ratio of low:high frequencies is given in Table 1. The R_p values are found to be acceptable when compared with those reported by other researchers [16]. The LSM-rich sample of 80 wt.% shows the highest R_p value of 0.919 Ω cm^2. As the LSM content is decreased, the R_p value decreases steadily to reach a minimum value of 0.315 Ω cm^2 at an LSM content of 50 wt.%, after which it increases steadily to reach a value of 0.756 Ω cm^2 at the lowest LSM content of 25 wt.%. The high-frequency arc shows a similar trend to the R_p value as the LSM content is decreased. The value of 0.171 Ω cm^2 at the highest LSM content of 80 wt.% decreases steadily to 0.120 Ω cm^2 at an

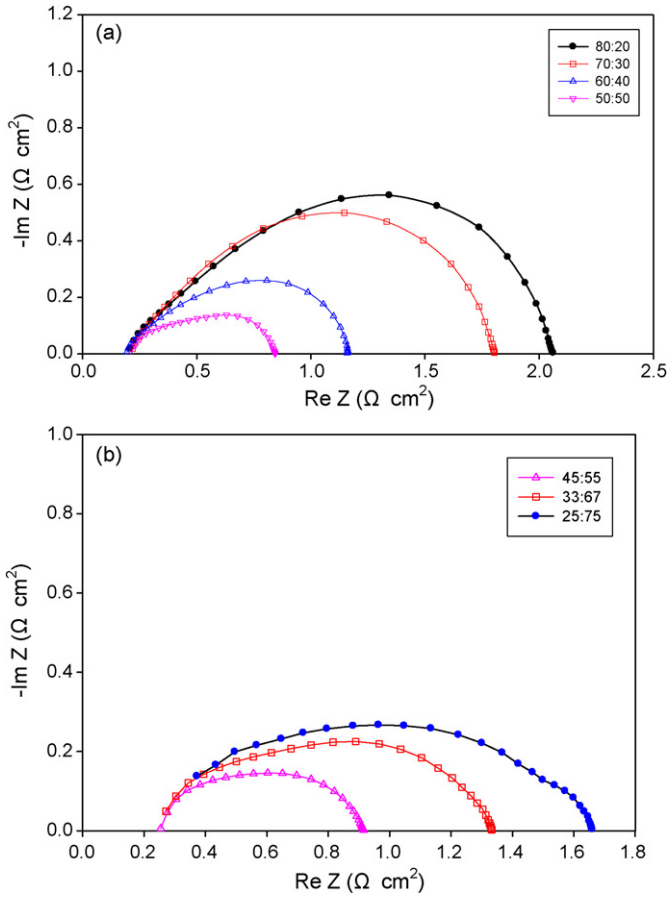

Fig. 5. Impedance spectra (EIS) of LSM–YSZ composite powders measured at 800 °C in air: (a) 80–50 wt.% of LSM content, (b) 45–25 wt.% of LSM content.

LSM content of 50 wt.%, after which it increases back to 0.599 Ω cm^2 at the lowest LSM content of 25 wt.%. Comparing the two frequency arcs, the low-frequency arc experiences a steady decrease as the LSM content decreases. The highest value of 0.748 Ω cm^2 is observed with the highest LSM content, and decreases to 0.636 and 0.337 Ω cm^2 as the LSM content is decreased to 70 and 60 wt.%, respectively. At an LSM content of 50 wt.%, there is a drop in the low-frequency arc down to 0.195 Ω cm^2, after which there is no appreciable decrease with further decrease in LSM content.

A number of researchers have suggested that each frequency part of the impedance spectra is related to some specific step of the oxygen reduction reaction or the microstructure of the electrode is related to TPB sites. Song and co-workers [15] have suggested that the high-frequency arc is related to YSZ phase interconnectivity, whereas the low-frequency arc is related to TPB site density [15]. Other groups suggest that the high-frequency arc is related to the charge-transfer resistance from the electrode|electrolyte interface into the electrolyte, and the low-frequency arc to the diffusion resistance [17,18]. Different interpretations may arise due to the observation that the states of the electrode, such as morphology, particle size and contact site, which are related to the electrochemical properties, are very sensitive to the synthesis method employed or to the material composition. Presently, LSM nanoparticles are synthesized *in situ* in a solution that contains dispersed YSZ particles. In this way, the aim is to deposit nanoparticles of LSM on the surface of YSZ particles. From the results in Table 1, the changing pattern of the low-frequency arc at various LSM contents suggests that it is, in fact, related to the TPB site and not to diffusion resistance. The highest resistance in the low-frequency arc can be observed at the highest LSM content, as agglomerated LSM particles and localized YSZ particles result in the lowest TPB site density. The TPB site density will increase with decrease in LSM content because of an improved inter-particle contact, which results in a decrease in the low-frequency arc. Until the LSM content is decreased to 50 wt.%, there exists an abrupt decrease in the low-frequency arc because nanoparticles of LSM have been dispersed on the surface of the YSZ particles. Thus, the trend of the TPB sites coincides with that of the low-frequency arc, not to the diffusion resistance, because the highest amount of pores (the lowest diffusion resistance) is observed at an LSM content of 50 wt.% in the present cathode case. From the changing pattern of the high-frequency arc in Table 1, it is suggested that this arc is related to charge-transfer resistance caused by either ionic or electronic conduction. At higher LSM contents in the cathode, the high-frequency arc is relatively high, indicating that the charge-transfer rate is very low due to localized YSZ limits on the ionic conduction. As the LSM content is decreased to 50 wt.%, the high-frequency arc reaches a minimum because of a good charge transfer in the cathode. With a further decrease in the LSM content down to 25 wt.%, the high-frequency arc increases back to saturation, and thereby indicates that the charge transfer is limited by electron transfer. This observation is due to the increased disconnection of LSM nanoparticles that are dispersed on the YSZ surface.

The last column in Table 1 shows the ratio of the low-frequency arc to the high-frequency arc. By taking the reciprocal value, this ratio is put in terms of conductive properties, that is, the conduction by the charge transfer divided by that due to the TPB site density. In other words, the ratio is charge transfer (oxygen ion conduction) efficiency of the TPB site, i.e.,

$$\frac{\text{low-frequency arc}}{\text{high-frequency arc}} = \frac{1/\text{high-frequency arc}}{1/\text{low-frequency arc}} = \frac{\text{charge transfer}}{\text{TPB site density}} = \text{charge transfer efficiency}$$

Reciprocal values of the low-frequency arc (the TPB site density) and the transfer efficiency of the TPB sites are plotted in Fig. 6. At the region of high LSM content (70–80 wt.%), the TPB site density stays very low because of the agglomeration of LSM particles and the disconnection of YSZ particles, both of which limit the ion conduction. The conduction efficiency, however, stays high because the cation conduction occurs only at a thin layer of the contact point between the cathode and the electrolyte layer, where the conduction rate

Table 1
Polarization resistance of LSM–YSZ composites at various LSM contents at 800 °C.

LSM:YSZ	R_p (Ω cm^2)	High-frequency arc (Ω cm^2)	Low-frequency arc (Ω cm^2)	Low-/high-frequency ratio
80:20	0.919	0.171	0.748	4.374
70:30	0.794	0.158	0.636	4.025
60:40	0.484	0.147	0.337	2.293
50:50	0.315	0.120	0.195	1.625
45:55	0.331	0.141	0.190	1.348
33:67	0.536	0.379	0.157	0.414
25:75	0.756	0.599	0.157	0.262

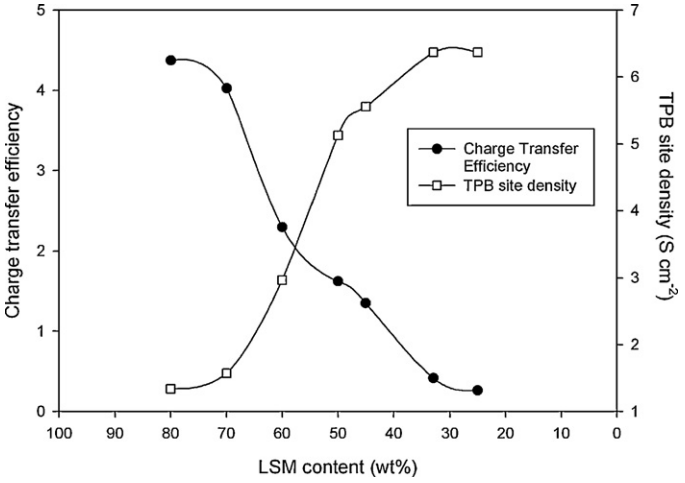

Fig. 6. TPB site density and charge-transfer efficiency of formed TPB sites as function of LSM content.

must be very high. As the LSM content decreases, the TPB site density is increased because of better phase connectivity between LSM–LSM, YSZ–YSZ and LSM–YSZ. Thus, the best microstructure is obtained at LSM contents of 45–50 wt.%, where the ion conduction rate is well balanced with the electron conduction. The transfer efficiency for this microstructure, however, is lower than that for the high LSM content, as shown in Fig. 6. With increased LSM content in the cathode, the conduction zone does not stay only at the contact point between the cathode and electrolyte layer, but extends to the deep cathode layer, where the conduction efficiency is low due to the concentration gradient of oxygen ions. At extremely low LSM contents (25–33 wt.%), the transfer efficiency of the TPB site stays very low because disconnections between LSM particles hinders electron transfer in the cathode layer and prohibits the conduction of the oxygen ions, even at the contact point between the cathode and the electrolyte layer.

The current (I)–voltage (V) curve and the power density of Ni–YSZ/YSZ/LSM–YSZ cells observed at 800 °C are shown in Fig. 7. Cell performance is measured for three button cells that have cathode materials of different compositions with an LSM content of 80, 50, or 25 wt.%. As expected, a maximum powder density of 791 mW cm^{-2} is observed with a 50 wt.% LSM content in the cathode. In comparison, the cell with a cathode of 25 wt.% LSM content shows similar power output to that with 80 wt.% LSM. From the results of impedance spectra, presented in Fig. 8, the R_p value of the

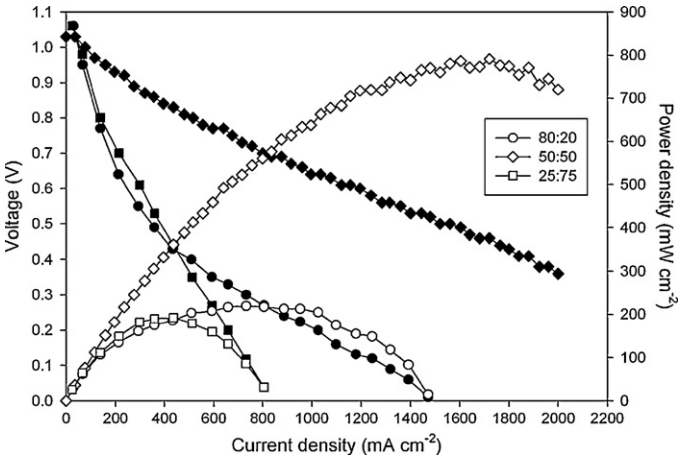

Fig. 7. Power density and I–V curves of NiO–YSZ/YSZ/LSM–YSZ cell at 800 °C: (□) 80 (○) 50 (◊) 25 wt.%.

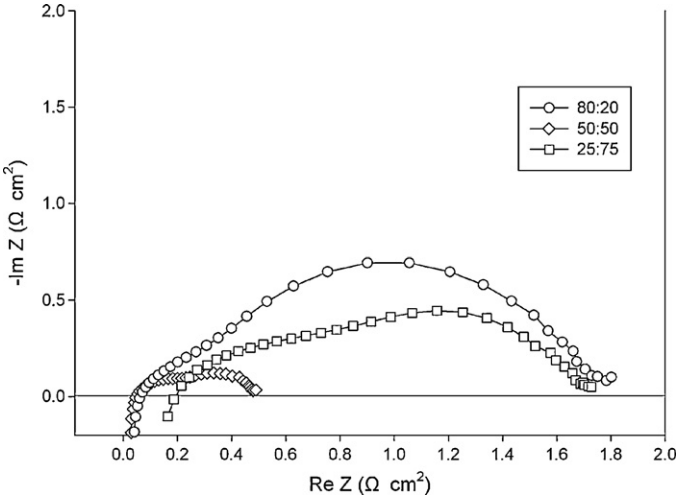

Fig. 8. Impedance spectra of NiO–YSZ/YSZ/LSM–YSZ cells under open-circuit voltage at 800 °C: (□) 80 (○) 50 (◊) 25 wt.%.

25 wt.% LSM content is lower than that of the 80 wt.% LSM, whereas the R_S value of the 25 wt.% LSM is higher than that of the 80 wt.% LSM. Therefore, the total resistance of these two cases would suggest that they would yield a similar power density. The lower R_p value of the 25 wt.% LSM content results from smaller particles of LSM. The higher value for R_S is caused by the extension of the electrolyte layer deep into the cathode layer, where rich YSZ particles form the electrolyte layer after being sintered, as shown in the SEM results of Fig. 4c.

4. Conclusions

In LSM–YSZ composite powders, only the junction of the LSM and YSZ particles can be an effective reaction site because of the poor ionic conductivity of LSM. To improve the reactivity of LSM–YSZ composite cathodes, it is necessary to form as many TPB sites as possible with good connections to the electrolyte layer through the YSZ particles and good connections to the current-collector through the LSM particles. The composite cathodes with various LSM contents were synthesized in YSZ-dispersed solution by using the cellulose–glycine method. Nanoparticles of LSM having crystal sizes of 20 nm, and particle sizes of 50 nm were synthesized and attached to YSZ particles. The powder sample with 50 wt.% content of LSM shows the most uniform distribution of particles and the best inter-particle connections. The cathode prepared with 50 wt.% LSM content exhibits a maximum power density of 791 mW cm^{-2} in a button cell of Ni–YSZ/YSZ/LSM–YSZ, and the lowest cathodic polarization resistance of 0.315 Ω cm^2.

From the results of EIS measurements, it is concluded that the high-frequency arc is related to charge transfer and the low-frequency arc to TPB site density. At high LSM contents in the cathode, the low-frequency arc is high because of low TPB site density, due to the LSM-rich phase. The high-frequency arc is also high in this cathode because of low charge-transfer rates, which are caused by the limitation in ionic transfer. As the LSM content is decreased to 50 wt.%, the low-frequency arc drops suddenly because of a sudden increase in TPB sites due to good inter-particle connections. The high-frequency arc reaches a minimum here because of good charge transfer in the cathode. With further decreases in the LSM content down to 25 wt.%, the low-frequency are continues to decrease because of increased TPB sites, due to nanoparticles dispersed on the YSZ surface. The high-frequency arc increases back from the minimum value at 50 wt.% LSM content, however, indicating that charge transfer is limited

by electron transfer, due to poor phase connectivity among LSM particles.

It is also concluded that the ratio of the low-frequency arc to the high-frequency arc could be considered to represent the efficiency of charge transfer of the TPB sites (cation conduction per TPB site). This value is highest at high LSM contents (70–80 wt.%) because the LSM-rich cathode and YSZ electrolyte layer form a conduction zone only at a thin layer of the contact points, where the charge-transfer rate of oxygen ions will be very high. The cell performance, however, is observed to be very poor because the number of TPB sites is very low in such a thin conduction zone. With decreased LSM content, the conduction zone can be extended deep inside the cathode layer, which overcomes decreased conduction efficiency per TPB site to exhibit a maximum power density at 50 wt.% LSM content. Further decreases in the LSM content down to 25 wt.% causes increases in the TPB sites, but is not able to overcome the decrease in the conduction efficiency due to poor phase connectivity among LSM particles. Neither is it effective for increased R_S values due to the sintering of YSZ particles in the cathode, which results in an eventual decrease in the power density.

Acknowledgements

The authors gratefully acknowledge support from the Brain Korea 21 project and from the New & Renewable Energy R&D Program (4.0003982.01) under the Ministry of Knowledge and Economy, Republic of Korea.

References

[1] T.Z. Sholklapper, H. Kurokawa, C.P. Jacobson, S.J. Visco, L.C. De Jonghe, Nano Lett. 7 (7) (2007) 2136–2141.
[2] C. Lu, T.Z. Sholklapper, C.P. Jacobson, S.J. Visco, L.C. De Jonghe, J. Electrochem. Soc. 153 (2006) A1115–A1119.
[3] D.E. Vladikova, Z.B. Stoynov, A. Barbucci, M. Viviani, P. Carpanese, J.A. Kilner, S.J. Skinner, R. Rudkin, Electrochim. Acta 53 (2008) 7491–7499.
[4] T. Tsai, S.A. Barnett, Solid State Ionics 93 (1997) 207–217.
[5] S. Vasseura, E. Dugueta, J. Portiera, G. Goglioa, S. Morneta, E. Hadova, K. Knızek, M. Marysko, P. Veverka, E. Pollert, J. Magn. Magn. Mater. 302 (2006) 315–320.
[6] V. Uskokovic, M. Drofenik, Mater. Des. 28 (2007) 667–672.
[7] V. Krivoruchko, T. Konstantinova, A. Mazur, A. Prokhorov, V. Varyukhin, J. Magn. Magn. Mater. 300 (2006) e122–e125.
[8] C.N. Chervin, B.J. Clapsaddle, H.W. Chiu, A.E. Gash, J.H. Satcher Jr., S.M. Kauzlarich, Chem. Mater. 18 (2006) 1928–1937.
[9] T.Z. Sholklapper, C.P. Jacobson, S.J. Visco, L.C. De Jonghe, Fuel Cells 08 (5) (2008) 303–312.
[10] W. Zhou, Z. Shao, R. Ran, H. Gu, W. Jin, N. Xu, J. Am. Ceram. Soc. 91 (4) (2008) 1155–1162.
[11] N.Q. Minh, J. Am. Ceram. Soc. 76 (1993) 563.
[12] H. Taimatsu, K. Wada, H. Kaneko, H. Yamamura, J. Am. Ceram. Soc. 75 (1992) 401.
[13] R. Chiba, Y. Tabata, T. Komatsu, H. Orui, K. Nozawa, M. Arakawa, H. Arai, Solid State Ionics 178 (2008) 1701–1709.
[14] J. Piao, K. Sun, N. Zhang, S. Xu, J. Power Sources 175 (2008) 288–295.
[15] H.S. Song, S. Lee, S.H. Hyun, J. Kim, J. Moon, J. Power Sources 187 (2009) 25–31.
[16] V.A.C. Haanappel, J. Mertens, D. Rutenbeck, C. Tropartz, W. Herzhof, D. Sebold, F. Tietz, J. Power Sources 141 (2005) 216–226.
[17] A. Mitterdorfer, L.J. Gauckler, Solid State Ionics 111 (1998) 185–218.
[18] H.Y. Lee, S.M. Oh, Solid State Ionics 90 (1996) 133–140.